Volume 1 | Number 1 | Jan 2013 | Pages 1–100

Journal of
Materials Chemistry C

Materials for optical and electronic devices
www.rsc.org/materialsC

ROYAL SOCIETY
OF CHEMISTRY
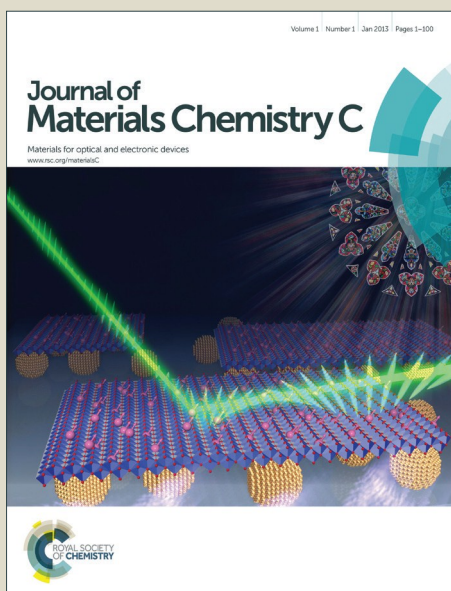
This is an *Accepted Manuscript*, which has been through the
Royal Society of Chemistry peer review process and has been
accepted for publication.

Accepted Manuscripts are published online shortly after
acceptance, before technical editing, formatting and proof reading.
Using this free service, authors can make their results available
to the community, in citable form, before we publish the edited
article. We will replace this *Accepted Manuscript* with the edited
and formatted *Advance Article* as soon as it is available.

You can find more information about *Accepted Manuscripts* in the
Information for Authors.

Please note that technical editing may introduce minor changes
to the text and/or graphics, which may alter content. The journal's
standard **Terms & Conditions** and the **Ethical guidelines** still
apply. In no event shall the Royal Society of Chemistry be held
responsible for any errors or omissions in this *Accepted Manuscript*
or any consequences arising from the use of any information it
contains.

Journal Name

ARTICLE

Improved output characteristics of organic thin film transistors by using an insulator/protein overlayer and their applications

Jinsung Choi, Hong Goo Jeon, O. Eun Kwon, Ingon Bae, Jaewon Cho, Yunki Kim, and Byoungchoo Park*

We herein present our study of the effect of an insulator/protein overlayer deposited onto semiconducting active layers in organic thin film transistors (OTFTs) with regard to their electrical performance. The active layers used were composed of 6,13-bis(triisopropylsilylethynyl)-pentacene (TIPS-PEN) blended with poly(α-methylstyrene) (PaMS), and the overlayer consisted of a bottom insulating (protecting) layer of an amorphous perfluoropolymer (Cytop) and a top protein layer of negatively charged bovine serum albumin (BSA). The functional layers were deposited using a simple solution-coating method which involved a horizontal dip coating process. We show that the Cytop/BSA overlayer on the TIPS-PEN:PaMS active layer improved the electrical performance of the OTFTs; the devices with the Cytop/BSA overlayer exhibited an average effective mobility of 0.25 cm^2 V^{-1} s^{-1}, which was higher than those of bare devices without any overlayer (0.20 cm^2 V^{-1} s^{-1}). This improved performance of OTFTs with the overlayer was successfully simulated and was found to stem from the formation of a second current channel in the TIPS-PEN:PaMS active layer via the electric field effect of the negatively charged BSA overlayer. These results demonstrate that OTFTs employing charged protein overlayers show considerable promise for the production of high-performance OTFT devices.

Introduction

Organic thin film transistors (OTFTs) have been studied intensively with regard to the development of organic materials and device structures with the goal of producing cost-efficient, lightweight, flexible, high-performance electronic devices.[1-9] In order to achieve such an end, researchers continue to direct their efforts toward performance and stability improvements without reducing the simplicity of the OTFT device fabrication process. The performance of OTFTs has been improved significantly in recent years; for example, some OTFTs now exhibit high mobility levels that are comparable to, or superior to, that of amorphous silicon thin film transistors in the range 0.5-1.5 cm^2 V^{-1} s^{-1}.[5-7] Due to their various advantages, including compatibility with plastic substrates and amenability to low-temperature fabrication methods, OTFTs can be applied in a range of areas, such as the pixel-switching elements used in active-matrix display devices and in electronic paper.[8,9] Furthermore, their ability to transduce a molecular binding event or a biological reaction directly into an electronic signal places OTFTs among the best electronic devices to use in accurate diagnostic sensing applications; i.e., any additional electric field induced by any bio- or chemical binding or reaction near the active layer in OTFTs can modulate the current flow through the active layer, resulting in organic

transistor-based sensors for real-time, label-free, portable, and disposable devices.[10-20]

Three different methods can be employed to fabricate such OTFTs: vacuum-evaporation deposition, the single-crystal growing method, and solution-processing.[1-23] Normally, the solution-processing of organic semiconductors offers a versatile and easy way to fabricate OTFTs.[1-5,11,12,15-19,23] However, the performance of solution-processed OTFTs is often not as good as that of equivalent devices fabricated using the single-crystal growing method[6,14] or vacuum-deposition methods[7-10,13-22] owing to the reduced crystalline ordering and poor uniformity found in solution-processed films.[24-26] A number of researchers have developed various processing techniques for organic semiconducting materials with the aim of establishing a greater degree of control over the thin-film deposition process. Examples of these efforts include the alignment of layers or the application of external fields,[24-26] the use of vitrification agents to control the crystallisation,[27] zone casting,[28,29] solvent vapour annealing,[30] a solvent treatment,[31] and zone refinement.[32] Another noteworthy approach is solution-processing using a polymer-blended small-molecular semiconductor, such as the small molecular 6,13-bis(triisopropylsilylethynyl)-pentacene (TIPS-PEN) semiconductor blended with the polymer poly(α-methylstyrene) (PaMS) (TIPS-PEN:PaMS).[33,34] In spin-coated TIPS-PEN:PaMS layers, the TIPS-PEN semiconductor and PaMS polymer simultaneously separate vertically to form a

trilayer structure, which can lead to good device performance.[33,34] Recently, thin TIPS-PEN:PaMS active layers were also fabricated by means of horizontal-dip (H-dip) coating, which is a well-known, advanced coating method for depositing a solution in a controlled fashion.[35,36] In contrast to the trilayer structure associated with spin-coated films, a graded structure with large polycrystalline TIPS-PEN domains was formed when an H-dip coating was used, resulting in improved OTFT performance with a maximum field-effect mobility of 0.20 cm^2 V^{-1} s^{-1}, a value which is much higher than those of spin-coated TIPS-PEN:PaMS OTFTs.[36] However, despite the recent development of various processing techniques, solution-processed OTFTs are still linked to relatively low device performance issues, such as a low current flow through the active layer in the OTFTs. Therefore, there remains a need to find a simple but effective way to enhance the performance of solution-processed OTFTs.

The aim of this study is therefore to improve the electrical performance of OTFTs, with the ultimate goal of achieving a simple and reliable fabrication method. On the basis of the sensing mechanism of OTFTs, we suggest a device configuration to increase the drain current flow by introducing charged protein-based overlayers into the OTFTs. We herein report the fabrication and characteristics of bottom-contact OTFTs covered by overlayers of a bottom insulating (passivating) layer of amorphous perfluoropolymer (Cytop)[37,38] and a top bio-molecular layer of the negatively charged protein bovine serum albumin (BSA).[39] The semiconducting active layers used were composed of H-dip-coated p-type TIPS-PEN:PaMS films. We herein show that the semiconducting TIPS-PEN:PaMS active layers covered by solid overlayers of Cytop/BSA exhibit an improved effective mobility of 0.25 cm^2 V^{-1} s^{-1}, which is higher than that (0.20 cm^2 V^{-1} s^{-1}) of the bare active layers in OTFTs. This type of structural arrangement of the active layers with the aforementioned overlayers can be used for the fabrication of various high-performance electrical and/or biological devices.

Experimental

Materials and Device Fabrication. For the bottom-contact OTFT devices, we used a 300-nm-thick layer of thermally grown SiO$_2$ as the gate dielectric on a heavily doped n-type (100) Si wafer substrate (0.05 Ohm cm). After routinely cleaning the wafer, Cr/Au (5 nm/60 nm) source and drain electrodes were deposited by thermal evaporation (at a base pressure below 2.7×10^{-4} Pa) through a shadow mask on the wafer substrate, with a channel length of 50 μm and a channel width of 1000 μm. Prior to the deposition of the active layer, the substrates were cleaned using UV ozone. A self-assembled monolayer of pentafluorobenzenethiol (Sigma Aldrich) was formed on the Au electrodes to improve the metal/organic contact.[36] Hexamethyldisilazane (Sigma Aldrich) was then spin-coated onto the substrate at 4000 rpm and baked at 125 °C for 10 min. The active layer was then solution-coated on the substrates from a blended solution using a simple solution-coating method of H-dip coating.[35,36] The blended solution used was a mixture of TIPS-PEN (Sigma Aldrich) and the polymer binder PaMS (Sigma Aldrich) (0.3:0.7 wt%), which were dissolved in toluene. A small volume of the solution (~6 μl) per unit coating area (1 cm × 1 cm) was fed into the gap of the cylindrical H-dip head using a syringe pump (NE-1000, New Era Pump Systems, Inc.). The height of the gap, h_0, was adjusted vertically and the carrying speed, U, was controlled by a computer-controlled translation stage (SGSP26-200, Sigma Koki Co., Ltd.). After a meniscus of the coating solution had formed on

the substrate, the substrate was transported horizontally such that the H-dip head spread the solution evenly on the transporting substrate while maintaining the shape of the downstream meniscus of the solution. The H-dip-coated TIPS-PEN:PaMS layers were then dried at 100 °C for 60 min using a heating plate in order to remove the remaining solvent.

Next, to protect the fabricated TIPS-PEN:PaMS OTFTs, we further coated an insulating overlayer of Cytop (Asahi Glass Co., Ltd.)[37,38] onto the TIPS-PEN:PaMS active layer using the H-dip coating method. The Cytop-coated TIPS-PEN:PaMS OTFTs were dried at 100 °C for 10 min. Next, in order to form top a solid BSA overlayer on the Cytop overlayer, *i.e.*, Cytop/BSA, we H-dip-coated an aqueous solution of BSA (50 μM) onto the Cytop-coated TIPS-PEN:PaMS active layer and dried the BSA overlayers under nitrogen gas.

Separately, to investigate the current flowing capability of the OTFTs, organic light-emitting devices (OLEDs) were prepared according to the following method. Glass substrates patterned with tin-doped indium oxide (ITO, 80 nm, 30 Ohm square^{-1}) were cleaned using a detergent solution, demineralised water, ultrasonication in acetone and isopropyl alcohol, followed by a UV-ozone treatment. The cleaned substrates were coated with a 40 nm-thick film of poly(3,4-ethylenedioxythiophene):poly(styrenesulfonic acid) (PEDOT:PSS; P VP AI4083, H.C. Starck) in ambient air and were annealed subsequently at 120 °C for 20 min. Single emissive layers of the light-emitting conjugated polymer known as Super Yellow (SY; Merck), a fluorescent poly(p-phenylene vinylene) co-polymer[40] were spin-casted onto the top of the PEDOT:PSS hole-injection layer under a controlled nitrogen atmosphere. Subsequently, a thin electron-injecting layer of cesium carbonate (2 nm) and an aluminium top cathode (~50 nm) were thermally evaporated (0.5 nm s^{-1}) under a vacuum (base pressure ~2.7×10^{-4} Pa). The effective size of the light-emitting area was 2.0 mm × 2.0 mm.

Characterisation. To evaluate the functional film quality of the fabricated TIPS-PEN:PaMS, Cytop, and BSA overlayers, we monitored topographic images of the surface morphologies of the films by means of atomic force microscopy (AFM, Nanosurf easyScan 2 AFM, Nanosurf AG Switzerland Inc.). The electric response of the OTFT device was recorded using a semiconductor parametric analyser with a source meter unit (Keithley 2400). Light emission from the OLEDs driven by OTFTs was also recorded simultaneously using a Chroma Meter CS-200 (Konica Minolta Sensing, Inc.).

Results and discussion

Device performance of TIPS-PEN:PaMS OTFTs fabricated by means of H-dip coating

Initially, we investigated the device performance of bottom-contact TIPS-PEN:PaMS OTFTs which were fabricated using a blended solution of TIPS-PEN and PaMS. The active TIPS-PEN:PaMS layer was deposited onto the Si wafer substrates from the blended solution using the simple solution-coating method of H-dip coating (see Figure 1(a)).[35,36] The thickness of the H-dip-coated TIPS-PEN:PaMS film can be described by the associated drag-out problem proposed by Landau and Levich,[41] in which the thickness (h) of the film obtained can be described using the well-known relationship[35,36] $h \propto (\mu U / \sigma)^{2/3} \cdot R_d$, where R_d represents the radius of the associated downstream meniscus. As shown in the figure, the thickness of the H-dip-
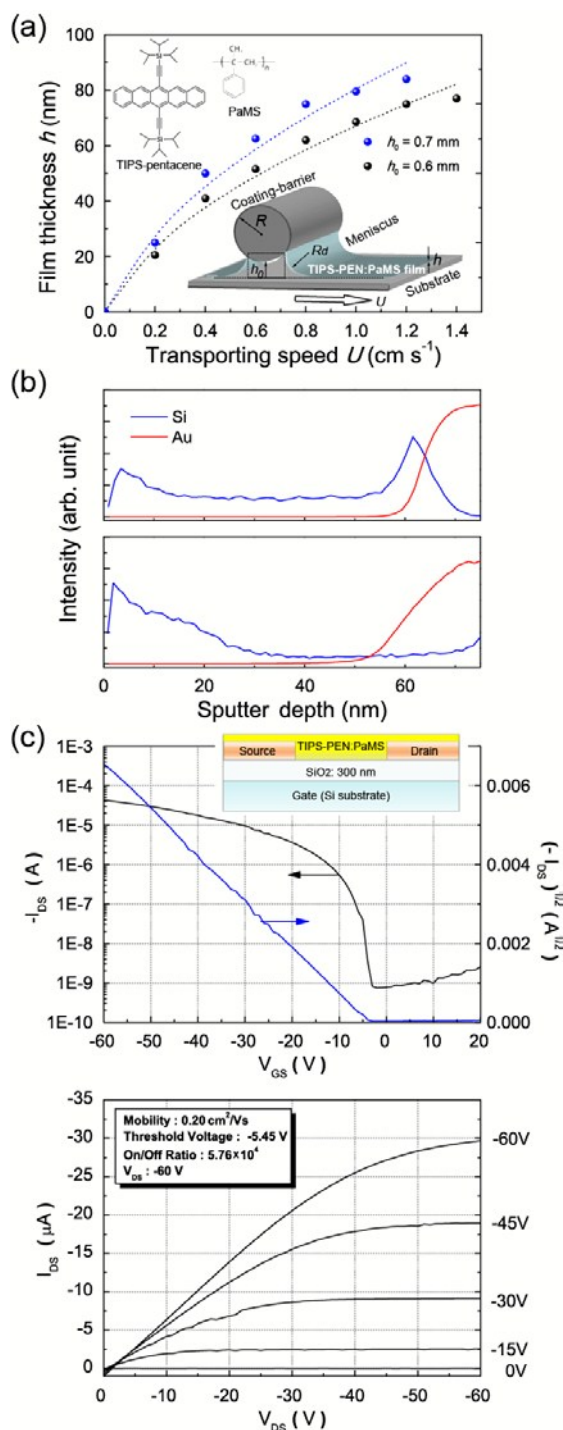
Fig. 1 (a) Thickness of the TIPS-PEN:PaMS film as a function of U for two h_0 measures. The solid curves show the theoretical predictions. The inset shows the chemical structures (upper) of TIPS-PEN and PaMS and a schematic illustration of the horizontal-dip (H-dip) coating process showing the coating barrier, a gap height of h_0, and a coating speed denoted by U. (b) Depth profiles of Si and Au ions in the spin-coated (upper) and H-dip coated (lower) TIPS-PEN:PaMS OTFTs. A sputter depth of zero was used at the top surface of the TIPS-PEN:PaMS film on the Au electrodes. (c) Transfer curves (upper) and output series (lower) measured for an H-dip-coated TIPS-PEN:PaMS OTFT device. The inset shows a schematic of an H-dip-coated TIPS-PEN:PaMS OTFT.

coated film is in good agreement with the theoretical value

predicted by the Landau-Levich relationship, as noted above, indicating that the nanoscale thickness of the H-dip coated film could be controlled by adjusting h_0 and U. In addition, for a better understanding of the active layer, we investigated the vertical distributions of the TIPS-PEN molecules in the H-dip-coated active layers using secondary ion mass spectrometry (SIMS). Figure 1(b) shows the vertical distribution of the Si ion as a marker of the TIPS-PEN molecule in the active layer and of the Au ion as a marker of the electrode of the OTFTs. In contrast to the trilayer structure (upper panel) in the spin-coated film, the H-dip-coated film shows a clear graded layer structure (lower panel), which may result in higher mobility and improved OTFT performance. As expected, notably, the H-dip-coated device exhibited a steep parabolic slope with regard to its transfer characteristics. It also showed a sharp turn-on point and excellent saturation behaviour in its output characteristics (also see representative the examples of $\sqrt{I_{DS}}$ and log (I_{DS}) vs. V_{GS} in Figure 1(c)). Hereafter, I_{DS} is used to denote the current between the source and the drain, V_{GS} is the gate voltage applied between the source and the gate, V_{DS} is the voltage between the source and the drain, V_{TH} is the threshold voltage, and the on/off current ratio is the ratio of the maximum and minimum drain currents at a given value of V_{DS}. The H-dip-coated OTFT had an average mobility of 0.20 cm^2 V^{-1} s^{-1} (a maximum mobility of 0.22 cm^2 V^{-1} s^{-1}), a threshold voltage of -1.62 V, and an on/off current ratio of 3.97×10^4 at a V_{DS} value of -60 V. This averaged value of the mobility of the H-dip-coated OTFT was similar to that (0.16 cm^2 V^{-1} s^{-1}) quoted in previous reports,[36] confirming that the blended system of TIPS-PEN with the PaMS polymer provides excellent OTFT device performance when the H-dipping process is used. The measured device performances of the H-dip-coated TIPS-PEN:PaMS OTFTs (the reference OTFT) are summarised in Table 1.

Device performance of TIPS-PEN:PaMS OTFTs in aqueous BSA solutions

With the H-dip-coated TIPS-PEN:PaMS OTFTs, we then observed the electrical performances of the OTFTs in aqueous media including bio-molecules of BSA protein, a commonly used model protein. The active TIPS-PEN:PaMS layer in these OTFTs was covered by a Cytop overlayer, which acts as an electrical insulator and a chemical protecting barrier against ions in an aqueous solution.[37,38] On the Cytop-overlayer-coated OTFT, a custom-built flow cell was constructed to confine the analyte solutions containing BSA, which was dissolved in deionised (DI) water (pH 5.7) at various concentrations, into the OTFT channel region, as shown in Figure 2(a). The contact area was approximately 1.0 mm × 1.0 mm and the flow channel was connected to a dispenser to deliver the solution from the reservoirs to the OTFT top surface at a constant volume of ~3 μl. The contact area was also connected to a small gas nozzle, blowing a stream of N$_2$ gas to remove the remaining solvent. In addition, several possible mechanisms can be considered with regard to the adsorption of BSA on the Cytop surface, e.g., the

hydrogen bonding interactions between the N-H of the BSA and the C-F chain of the Cytop,[42] hydrophobic interactions,[43] physical adsorption, and others. Among these, the hydrogen bonding interaction between BSA and Cytop is weak in water due to hydration in water, while the hydrophobic interaction is also negligible because the surface of BSA is negatively charged and thus hydrophilic. Hence, physical adsorption may be the driving force of the non-specific BSA adsorption, and device surfaces can be fully recovered by rinsing then with pure water. Thus, the occurrence of the adsorption of BSA on the Cytop-deposited OTFT may be converted to a current response (I_{DS}) of the device, which ultimately depends on the BSA composition and concentration.[38,44]

For stable device operation of the OTFTs in aqueous media, the Cytop-deposited OTFT in the BSA solution was operated at low V_{DS} and V_{GS} values with four steps for monitoring the OTFT response. A brief description of each step of the *in-situ* monitoring process follows: step 1: Recording of the OTFT response to DI water (~3 µl) dropped on the Cytop-coated OTFT for ~1 min (water level). Step 2: Recording of the response to air on the dried Cytop-coated OTFT by means of an exposure to pure N$_2$ gas for ~1 min (air level). Step 3: Recording of the response to the BSA solutio n (~3 µl) at a given concentration dropped onto the channel region of the Cytop-coated OTFT. Step 4: Recording of the response to the removal of the BSA solution on the Cytop-coated OTFT by flowing DI water with a successive exposure to N$_2$ gas for ~1 min as a cleaning process. Figure 2(b) shows the *in-situ* measurement of I_{DS} vs. time using a Cytop-coated TIPS-PEN:PaMS OTFT at a constant bias (V_{GS} = -3 V and V_{DS} = -3 V) with four monitoring OTFT response steps over time. As shown in the figure, prior to the analyte injection, the baselines of I_{DS} (water and air levels) were recorded during steps 1 and 2, after which a BSA solution (50 µM) was injected and changes in the I_{DS} value were observed during step 3 compared to the baseline values. It is clear from the changes in I_{DS} that the polarity of water or BSA molecules on the Cytop surface plays a central role through the creation of charge carrier traps. Due to the isoelectric point (pI) of 4.7 for BSA, the amino acids of BSA in DI water at 25 °C show negative charges;[39] thus, intuitively, one may anticipate a decrease in the current upon the adsorption of BSA onto the Cytop-coated TIPS-PEN:PaMS OTFT, as it pulls charge carriers (holes) away from the bottom channel region formed near the interface between the bottom insulating layer of SiO$_2$ and the TIPS-PEN:PaMS active layer, in a manner similar to that described in the literature.[38,44] However, such anticipation of a decrease in the current is clearly inconsistent with this observation of the sensing behaviours. It was noted that when the BSA solution was removed by the cleaning process with the DI water and N$_2$ gas during step 4, the current nearly returned to its original value (air level), indicating that the binding or adsorption of the BSA on the Cytop overlayer is not strong. Thus, the observed device performance described above shows that the fabricated transistors were stable in water and functioned well even in
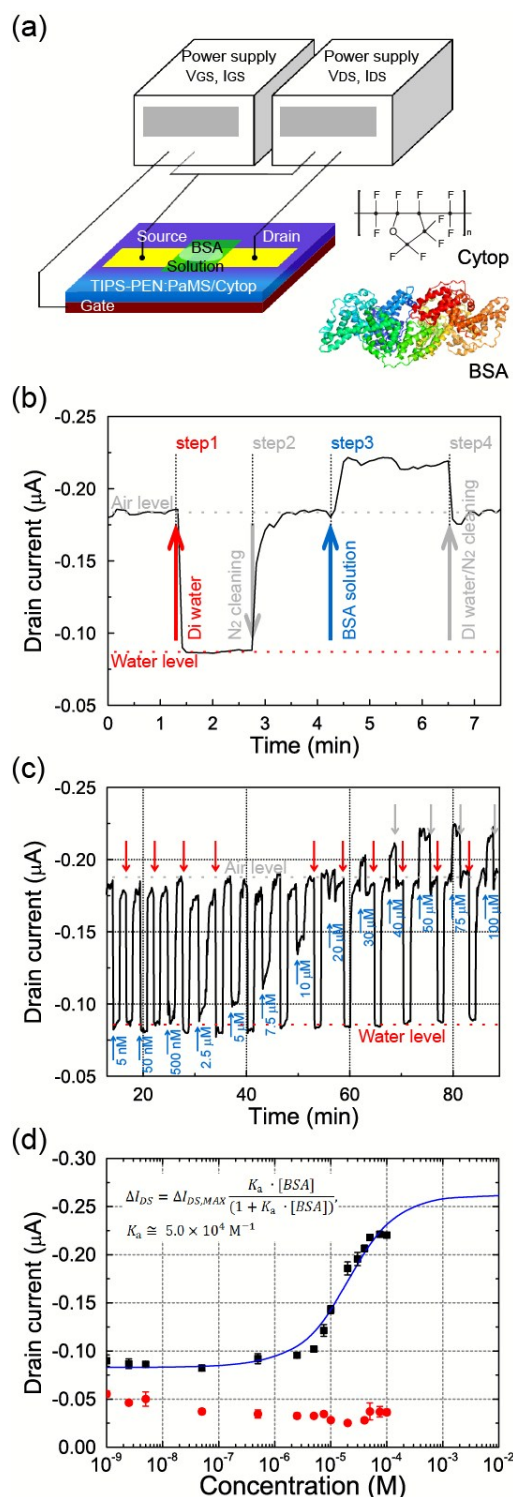

Fig. 2 (a) Schematic of an H-dip-coated OTFT operating in aqueous BSA solutions. (b) *In-situ* monitoring of changes in the drain current of the OTFT device for four processing steps, 1-4, with an aqueous BSA solution (50 µM, pH 5.7). (c) Changes in the drain current of the OTFT device as a function of the concentration of BSA in solutions (pH 5.7) for multiple adsorption cycles separated by the water/N$_2$ rinsing process. (d) Quantitative OTFT response curves of BSA binding isotherms on the OTFTs shown in (c). The solid curves show the best fit of the Langmuir isotherm. Red circles show the OTFT response for the BSA solutions at pH 3.

aqueous solutions when monitoring the binding of proteins on a Cytop surface in terms of the current change (I_{DS}).

Next, for more details on the considerable changes in the current upon the adsorption of the BSA on the OTFT, we observed the I_{DS} responses of devices with BSA solutions at various concentrations ranging from 5 nM to 100 μM. Figure 2(c) shows the device responses as monitored by measuring the changes in I_{DS} over time for multiple adsorption cycles separated by the DI water/N_2 rinsing process (step 4). It is clear from the figure that the measured I_{DS} value started to increase with an increase in the concentration of BSA with a detection limit of about 1.21 μM, as determined using an analytical method,[17] until reaching the saturation point at bulk concentrations of about 50-100 μM during the exposure to the BSA solution (step 3), while the current levels returned to their original points at every cleaning step. Remarkably, upon the introduction of the BSA solution at a concentration that exceeded 20 μM onto the Cytop-coated device, we clearly observed that the values of I_{DS} became higher than those of the air level . The highest concentration of BSA investigated here was 100 μM, as a further increase in the concentration resulted in too high a viscosity of the solution to apply it onto OTFTs.

For the BSA solutions used, we also found that the pHs of the BSA solutions had increased slightly from 5.5 to 7.2 with an increase in the BSA concentration. By varying the pH from 5.5 to 7.2, which is higher than that of the pI of BSA, the BSA became highly negatively charged in its aqueous solution.[39] Thus, the accumulation of the negative charge density on the surface of the Cytop-coated OTFT induces positive charges (holes) in the TIPS-PEN:PaMS active layer at the interface between the Cytop insulating overlayer and the active layer, according to the field effect. Thus, one may expect the observation that the current response decreases as a result of the disturbance of the hole accumulation process at the bottom channel near the SiO_2 insulating layer in the p-type OTFT used, as mentioned above. Such a trend in the responses of decreased drain currents has been also observed for the detection of small molecules,[45] DNA oligomers,[11] and ions[46] using OTFT-based sensors. However, interestingly, by increasing the negatively charged BSA concentration, we clearly observed an opposite current response in our OTFT, as shown in Figure 2(c).

In order to observe the behaviours of the current response more closely, the device responses, shown in Figure 2(c), were replotted as a function of the BSA concentration in Figure 2(d). In this figure, the plot of the device response vs. the BSA concentration was analysed using a Langmuir isotherm model.[38,47] The blue curve in the figure shows the Langmuir fit. Application of this analytical model yields an association constant (K_A) of about 5.0×10^4 M^{-1}, which is one order of magnitude smaller than that of an anti-BSA-protein according to thermally evaporated pentacene transistor-based sensors.[38] It was noted that the maximum surface coverage of BSA on the Cytop-coated OTFT obtained from the analysis was about 83% of the full surface coverage. In addition, we compared the current responses of OTFTs with a BSA solution at pH 3 (red circles in Figure 2(d)), finding that the current response did not
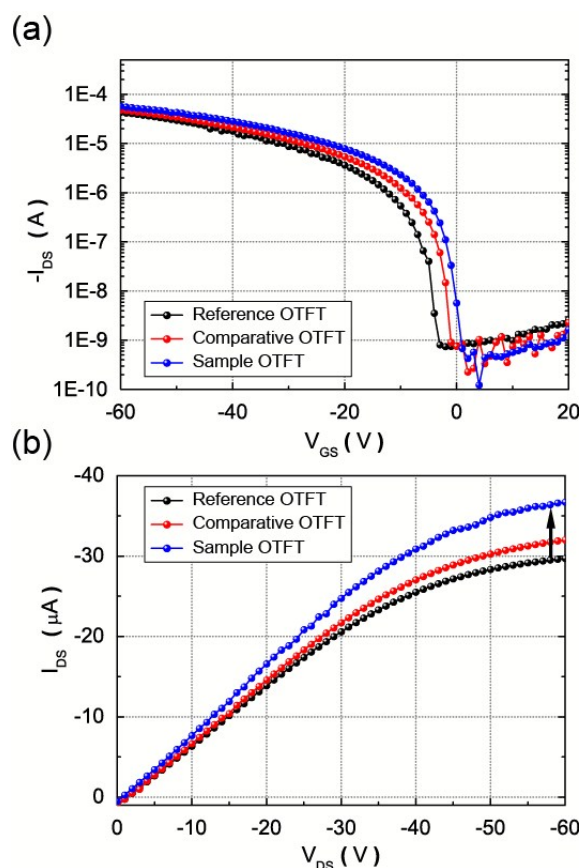
Fig. 3 Changes in the transfer curves (a) and output series (b) measured from H-dip-coated TIPS-PEN:PaMS OTFTs for the formation of dried overlayers on the TIPS-PEN:PaMS active layer in air (Black: bare reference OTFT without any overlayer, Red: OTFT with Cytop overlayer, and Blue: OTFT with the Cytop/BSA overlayer).

increase even at a high concentration of BSA in a solution at pH 3, in which the BSA became highly positively charged in the solution due to its lower pH compared to that of the pI of BSA. Thus, it is clear that the polarity of BSA plays a central role in the increased current responses of OTFTs in BSA solutions. The sensing performance of the OTFTs investigated is summarised in Table 2. In the table, we also compare the device performances of several pentacene-based OTFT sensors reported previously,[10,20,38,44] indicating that our OTFT device may be applied as a sensitive and reproducible sensor, especially for the selective detection of negative charged proteins or biomolecules with a wide range of response.

Electric performance of TIPS-PEN:PaMS OTFTs with solid Cytop/BSA overlayers in air

Upon the introduction of BSA onto the Cytop-deposited OTFT device at a high concentration, an increased I_{DS} was clearly observed for the BSA solutions at pH 5.7. From these results, we presumed that the dual-gate field effect[46,48,49] became more pronounced in our OTFTs when the concentration of BSA reached some threshold limit, acting as a top gate. In order to assess the possibility of an improvement in the device

performance, we measured the electric characteristics of TIPS-PEN:PaMS OTFTs with a Cytop overlayer and OTFTs with a solid Cytop/BSA overlayer in air. To form the overlayers on the OTFTs, Cytop and BSA solutions were coated onto bare OTFTs without any overlayer (reference OTFTs) and were dried subsequently under N_2 gas. A summary of the measured results is also given in Table 1. The reproducibility of this fabrication process was tested using six different OTFTs prepared with the same procedure for each condition, after which we obtained average values for the devices. In all OTFT samples, the device response of the OTFTs with the Cytop/BSA overlayer showed improved electrical performance levels, as indicated in Table 1. Figure 3 shows typical examples of $\sqrt{I_{DS}}$ and $\log (I_{DS})$ vs. V_{GS} when V_{DS} = -60 V and the I_{DS} vs. V_{DS} outcome of the OTFTs with the Cytop/BSA overlayers. After the formation of the BSA overlayers, the transfer and output characteristics clearly improved compared to those before the formation of the overlayer, providing evidence of the effectiveness of the BSA protein overlayer on the TIPS-PEN:PaMS active layers. Notably, the sample device with the Cytop/BSA overlayer had an average effective mobility of 0.25 cm^2 V^{-1} s^{-1} (a maximum effective mobility of 0.31 cm^2 V^{-1} s^{-1}), a threshold voltage of 1.26 V, and an on/off current ratio of 1.41×10^5 when V_{DS} = -60 V (see Table 1). This average effective mobility value for the OTFTs with the Cytop/BSA overlayer was higher than those of the reference OTFT without any overlayer (0.20 cm^2 V^{-1} s^{-1}) and higher than those of OTFTs with a Cytop overlayer. This result shows that the TIPS-PEN:PaMS active layers can provide improved device performance when an appropriate protein overlayer is introduced. We assume that the increments in the drain current and the effective mobility arise mainly because the negatively charged BSA overlayer on the TIPS-PEN:PaMS active layer may have induced additional current flows without disturbing the existing bottom channel which had formed near the bottom SiO_2 insulator layer due to the bottom-gate OTFT geometry. Hence, the drain current flowing through the channels may have increased compared to the reference OTFT without an overlayer. A doping effect on the TIPS-PEN:PaMS active layer by the overlayers is another possible cause of the increment in the drain current and mobility.[50,51] It is also important to note that even when the BSA solution at pH 3 was used for the formation of a dried BSA overlayer on a Cytop-coated OTFT, the device performance thus obtained was similar to that of an OTFT with a Cytop/BSA overlayer fabricated with the BSA solution at a pH of 5.7 (Table 1), indicating that the contribution of the activity of hydrogen (acidity) or hydroxide (basicity) ions in the solutions may be negligible in the dried solid BSA films.

Film quality of the fabricated solid Cytop/BSA overlayers

Next, for a detailed understanding of the quality of the solid overlayers on the OTFTs, we investigated the surface morphologies of TIPS-PEN:PaMS, Cytop, and BSA layers by means of atomic force microscopy (AFM). Figure 4(a) shows
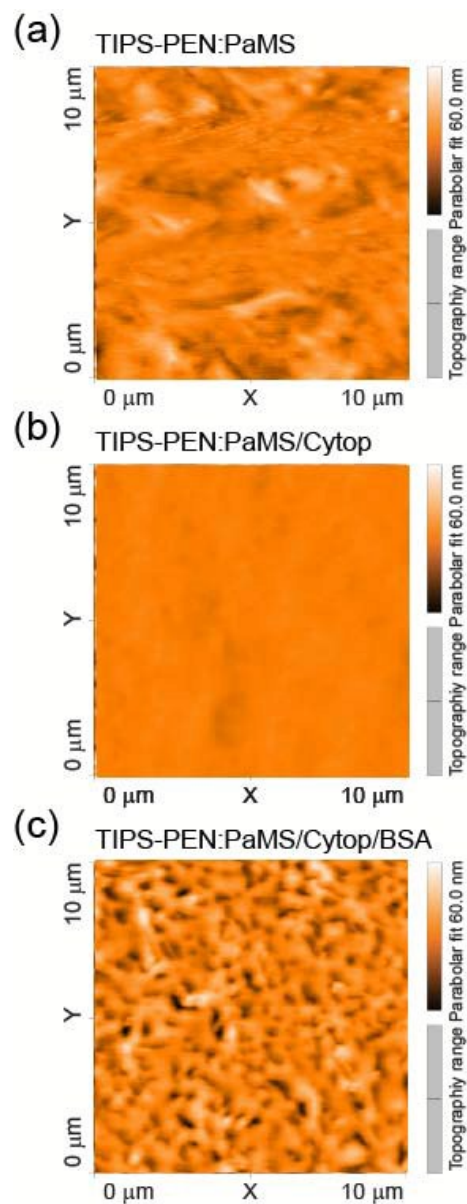
Fig. 4 10 μm× 10 μm AFM topographic images of the TIPS-PEN:PaMS (a), TIPS-PEN:PaMS/Cytop (b), and TIPS-PEN:PaMS/Cytop/BSA films (c).

the surface morphology of a 10 μm × 10 μm scan of part of an H-dip-coated TIPS-PEN:PaMS film. From the figure, it is clear that the H-dip-coated TIPS-PEN:PaMS layer is fairly smooth, with a root mean square (RMS) roughness of 4.46 nm, which is nearly double that of the spin-coated film, indicating large domain growth and related microstructural packing of the H-dip-coated TIPS-PEN:PaMS films. Figures 4(b) and 4(c) show AFM images of the bottom Cytop and the Cytop/BSA overlayers on the H-dip-coated TIPS-PEN:PaMS layers, respectively. As shown in the figures, both the Cytop and the Cytop/BSA overlayers are smooth, and the RMS surface roughness levels of the overlayers become 0.94 and 6.60 nm, respectively, indicating fairly homogeneous and uniform film structures of the overlayer formed on the TIPS-PEN:PaMS active layer.

Numerical simulations of the electrical performance of TIPS-PEN:PaMS OTFTs with Cytop/BSA overlayers

Given the impressive electrical performance and film quality levels of the functional layers, we undertook computer simulations of the current-voltage characteristics of TIPS-PEN:PaMS OTFTs considering the BSA layer as a upper overlayer generating an electric field and the Cytop layer as a lower insulating overlayer on the TIPS-PEN:PaMS active layer. In order to understand the cause of the improvement in the electric performance, we initially estimated the electrostatic potential of BSA protein molecules to create a simple model of BSA overlayer using the CHARMM-GUI tool, an academic research programme which is used widely for macromolecular mechanics and dynamics.[52] Figure 5(a) shows the electrostatic potentials of the surfaces 1 Å away from the BSA surface in water (dielectric constant: 80) and dielectric film (dielectric constant: 2.1 for BSA) environments, as obtained by solving the Poisson-Boltzmann equation.[53] The surface potential of the BSA ranges from -30 kT/e to +30 kT/e (*i.e.*, from -0.78 to +0.78 V), as shown in red and blue in the figure, giving an average surface potential of -0.07 V on the Cytop surface due to the excessive negative charges (17 components) of the BSA. Thus, it is expected that the charged terminations of BSA attached to the Cytop-coated OTFT influence the changes in the drain current via an additional electric field effect on the TIPS-PEN:PaMS active layer.

Next, in order to estimate the effect of the Cytop/BSA overlayers on the current-voltage (*I-V*) characteristics of the TIPS-PEN:PaMS OTFTs, simulations were performed using the 2D simulation package ATLAS (Silvaco International).[54] In these simulations, we considered an OTFT configuration based on a bottom contact device structure with a TIPS-PEN:PaMS active layer, as shown in Figure 5(b). The Cytop and BSA overlayers were considered as an insulator layer and a charged insulator layer, respectively, and the surface charge density due to the BSA on the Cytop surface was used as a fitting parameter in the simulations. Other detailed numerical descriptions of the parameters used in these OTFT simulations are also summarised in Table 3. For comparative purposes, we also simulated two other OTFTs using the configurations of a TIPS-PEN:PaMS OTFT without an overlayer (reference OTFT) and a TIPS-PEN:PaMS OTFT with a single Cytop overlayer (comparative OTFT). In these simulations, the functional layers in the OTFTs were considered to have the following fixed thicknesses: TIPS-PEN:PaMS layer: 80.0 nm, Cytop: 25.0 nm, and BSA: 10.0 nm. Because all of the variables are fixed apart from the structure of the overlayers, the electric performance is directly related to the overlayers used for the OTFTs.

The simulated *I-V* characteristics of the OTFTs are shown in Figure 5(c). It is clear from the figure that the simulated *I-V* values of the OTFT models are in good agreement with the experimental results, indicating that the BSA overlayer, acting as a charged insulator layer, induces an increase in I_{DS} and that the OTFT device is highly sensitive to the charges on the top surface of the device. In the simulation results, we obtained a

surface charge density ($Q_{induced}$) of -4.0 × 10^10 cm^-2, as induced by the BSA overlayer on the Cytop surface, which is comparable to the charge density Q_{BSA} (-8.11 × 10^10 cm^-2 for 83% surface coverage of BSA) estimated from the relationship[46] of $Q_{induced} = \Delta V_{TH} \cdot C_{SiO2}$ with the average shift in the threshold voltage (ΔV_{TH} = -1.36 V, Fig. 3(a)) and the capacitance (C_{SiO2} = 11.5 nF·cm^-2) of the bottom SiO₂ gate dielectric layer used. Moreover, the estimated surface charge density $Q_{induced}$ provides information about the effective voltage applied to the top Cytop capacitor C_{Top} (71 nF·cm^-2), i.e., a V_{Top}
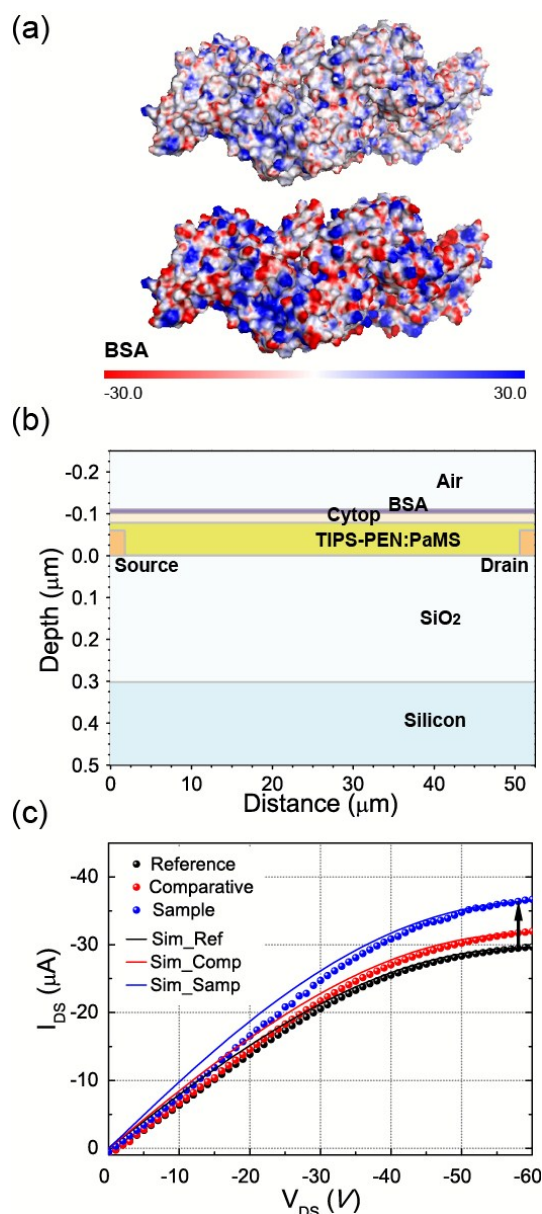

Fig. 5 (a) Calculated electrostatic potentials of the BSA surfaces in DI water (upper) and a BSA film (lower) according to the CHARMM-GUI programme. (b) Cross-sectional device structure of the OTFT employing the Cytop/BSA overlayer when used in the ATLAS simulation programme. (c) Plot of the experimental (circles) and simulated (curves) output characteristics of the OTFTs studied (Black: bare OTFT without an overlayer, Red: OTFT with the single Cytop overlayer, and Blue: OTFT with the Cytop/BSA overlayer).

(= $Q_{induced}$ /C_{Top}) value of about -0.09 V, which is also close to the average surface potential due to the BSA (-0.07 V), as estimated from the Poisson-Boltzmann equation. It was noted that the zeta potential values (-15 mV ~ -52mV) of the BSA for pH values in a range of 5.5-7.2, reported previously,[55] also confirm that both the effective voltage V_{Top} and the average surface potential are reasonable, implying that I_{DS} is significantly increased by introducing overlayers with large zeta potentials onto OTFTs. From these simulations, it can be confirmed that the OTFT with the Cytop/BSA overlayer exhibited improved output characteristics with sharper increases in the *I-V* curves and higher current flows than those of the other samples (with the single Cytop overlayer and without an overlayer). This result also indicates noticeably

Fig. 6 The simulated 2D hole-current density profiles in the TIPS-PEN:PaMS layers contacted with air (a), Cytop overlayer (b), and Cytop/BSA overlayers (c) on top of the TIPS-PEN:PaMS active layer in OTFTs according to the ATLAS programme.

better control and a higher flow of the hole-current through the active layer in the OTFT with the Cytop/BSA overlayers compared to the other samples, especially with regard to the reference OTFT without an overlayer. On the other hand, the slight increment in the drain current of the OTFT with the single Cytop overlayer can be explained in terms of the doping effect; i.e., the Cytop overlayer may cause an increase in the doping density of the TIPS-PEN:PaMS active layer.[50,51] When the doping density of TIPS-PEN:PaMS increases from 4.8 × 10^{15} cm^{-2} to 5.2 × 10^{15} cm^{-2}, the simulation results are in reasonably good agreement with the experimental results, similar to previous reports on an insulating/protecting overlayer.[50,51]

For a better understanding of the high current flows through the active layer in the OTFTs with the Cytop/BSA overlayers, we also simulated 2D hole-current density profiles in the active layers based on the OTFT configuration shown in Figure 5(b). The hole-current density profiles obtained in the simulation of the active layers in the OTFTs when V_{DS} = -60 V and V_{GS} = -60 V are shown in Figure 6. Figure 6(a) shows the simulated results for the reference OTFT without an overlayer. In this figure, it is clear that the hole-current density in the bottom channel formed by the bottom-gate voltage (V_{GS} = -60 V) decreases gradually with an increase in the distance from the bottom gate. The simulated profile shown in Figure 6(b) for the OTFT with the single Cytop overlayer is similar to that of the reference OTFT, but the channel height shows a slight increase owing to the increased doping density caused by the doping effect of the Cytop,[50,51] as mentioned above. On the other hand, as shown in Figure 6(c), the hole-current density profile in the active layers for the OTFT with the Cytop/BSA overlayer shows higher current densities than the other samples, extending not only to the normal bottom channel but also to a new top second-current channel.[46,48,49] Note that the top current channel formed in the active layer is mainly caused by the negatively charged BSA overlayer, which was not observed in the reference and comparative OTFTs. Thus, it is clear that in the case of the OTFT with the Cytop/BSA overlayer, the electric field induced by the BSA layer creates a new top second-current channel in addition to the normal bottom current channel near the bottom gate; i.e., dual channels are formed on both top and bottom sides of the TIPS-PEN:PaMS active layer. Thus, it is clear that the use of negatively charged BSA protein overlayers on p-type OTFT devices with a bottom contact configuration can result in a greater overall electrical performance level of OTFTs. These simulated results were consistent with our initial assumptions that the use of BSA, possessing negative charges above the pI, results in an increase in the value of I_{DS}.

Next, we want to comment on the comparison of our OTFTs with others reported previously.[38,44] In previous reports, the adsorption of negatively charged BSA onto the pentacene active layer in conventional OTFTs showed a decrease in the I_{DS} value,[38,44] which is in contrast to our observations of H-dip-coated TIPS-PEN:PaMS OTFTs with Cytop/BSA overlayers. In order to explain this discrepancy, we compared the vertical
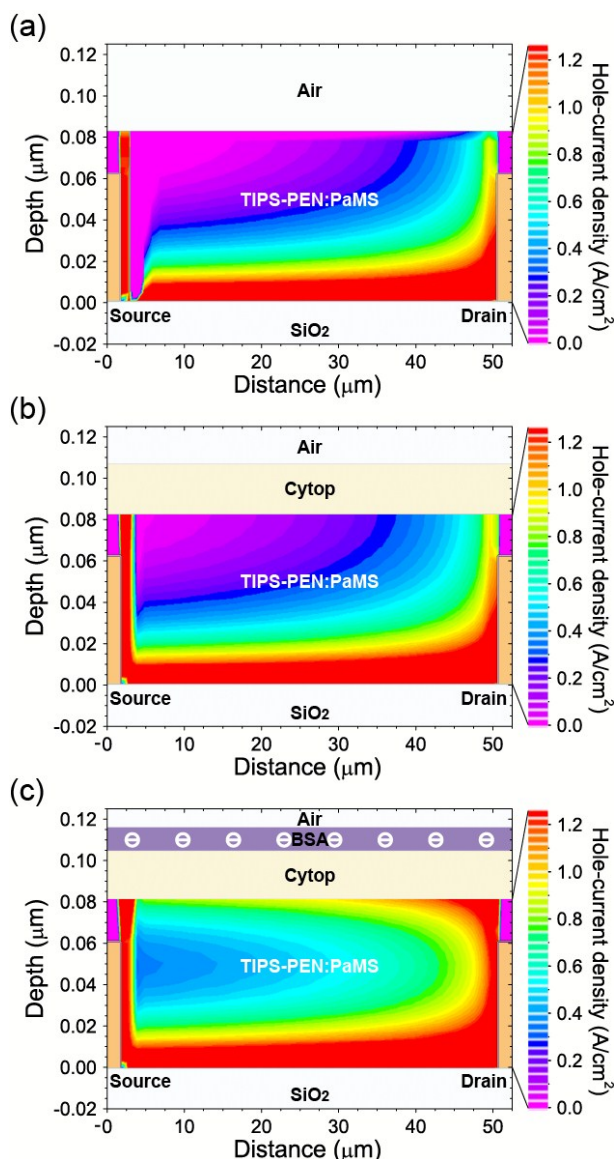
layer structure of the H-dip-coated active layer with those of the conventional layer in OTFTs. In the H-dip-coated layer, we recalled the vertically graded TIPS-PEN layer structure (see Figure 1(b)). We assume that the high concentration of TIPS-PEN found on the top surface of the active layer may be more favourable compared to that in other materials other materials for forming dual-current channels, increasing the value of I_{DS} in the OTFT. Thus, it can be suggested that the TIPS-PEN:PaMS active layer with a vertically graded structure is one of the main reasons why the H-dip-coated OTFT shows such a large increase in I_{DS} due to the adsorption of negatively charged BSA proteins. However, the exact mechanisms of the increases in the current are still not fully understood at this stage.

In additional simulation results, we found that the thickness of the Cytop overlayer had minor influences on the changes in the effective mobility of the TIPS:PEN active layer. This result was confirmed from experiments in which we fabricated a single BSA overlayer directly on the TIPS-PEN:PaMS active layer. In this case, the OTFT with the BSA overlayer gave the nearly the same electrical performance as that of the OTFT with Cytop/BSA overlayer, as also shown in Table 1. Thus, it is also clear that one can also fabricate efficient OTFTs using a single BSA overlayer, but the direct coating of an aqueous BSA solution on a TIPS-PEN:PaMS active layer may lead to device fabrication failure due to the lack of a protecting layer. More details of the Cytop thickness dependence will be reported elsewhere.

Applications of TIPS-PEN:PaMS OTFTs with a Cytop/BSA overlayer

Finally, we provide an application of the H-dip-coated OTFTs with the Cytop/BSA overlayer as studied here in an effort to investigate the current flowing capability of OTFTs to drive organic light-emitting devices (OLEDs), as shown in Figure 7. Here, the OTFTs used were prepared with a channel width of 3000 μm, and the OLEDs were fabricated with a light-emitting layer of SY.[40] It is clear from the figure that much brighter electroluminescent light was emitted from the OLED driven by the OTFT with the Cytop/BSA overlayer (lower panel) compared to that without an overlayer (upper panel). For a V_{DS} of -60 V and a V_{GS} of -60 V, the current density flowing through the OLED, driven by the Cytop/BSA-deposited OTFT, was as high as 1.75 mA cm^{-2} while the brightness of the device was about 180 cd m^{-2}, with a current efficiency of about 10.2 cd A^{-1}. In contrast, the current density flowing through the OLED driven by the OTFT without an overlayer was about 0.5 mA cm^{-2} and the brightness was only approximately 32 cd m^{-2}, with a current efficiency of about 6.4 cd A^{-1}. Interestingly, both the brightness and the efficiency were significantly greater for the OLED driven by the OTFT with the Cytop/BSA overlayer. These improved brightness and efficiency values can likely be attributed to the increased hole-current flows through the BSA-modified OTFT and thus the improved hole-electron balance in the EML recombination zone in the OLED. From this application, it can be concluded that the H-dip-coated TIPS-
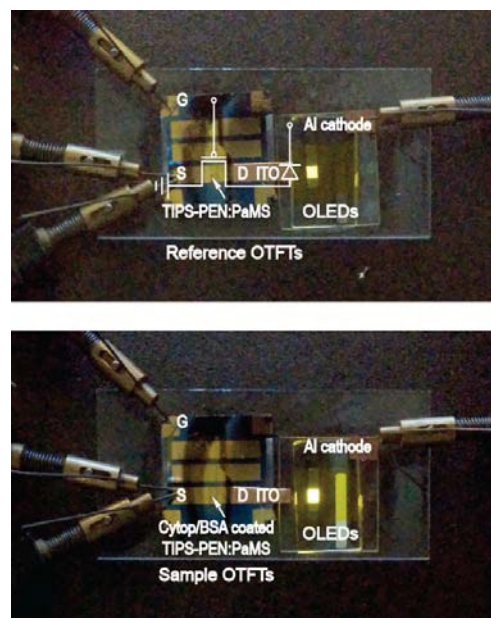
Fig. 7 Images of the operation of integrated OLEDs (right) driven by OTFTs (left) without (reference OTFT, upper panel) and with a Cytop/BSA overlayer (sample OTFT, lower panel). The active area of the OLED was 2.0 mm × 2.0 mm. The designed circuit diagram of the integrated OTFT and the OLED is also shown in the upper panel.

PEN:PaMS film covered with the Cytop/BSA overlayer shows considerable promise for the fabrication of high-performance OTFTs.

All of the foregoing results clearly demonstrate that the remarkable electrical performance of the H-dip-coated TIPS-PEN:PaMS OTFTs with Cytop/BSA overlayers show considerable promise for the fabrication of high-performance OTFTs. To the best of our knowledge, this is the first demonstration of high-performance p-type OTFTs modified by top overlayers of negatively charged proteins. Furthermore, the formation of other overlayers of charged materials, such as bio-molecules and/or polymer electrolytes on the active layer, can also be applied to the design of new organic electronic devices. Combining the described OTFTs with the roll-to-roll method of processing as reported in the literature will certainly lead to the development of inexpensive, fast, large-area, high-performance OTFT devices.

Conclusions

In summary, we have herein described the simple formation of overlayer on an H-dip-coated TIPS-PEN:PaMS active layer in p-type OTFTs, thereby allowing an enhancement of the electrical performance of the OTFTs. The overlayers consist of a bottom insulating Cytop layer and a top negatively charged BSA protein layer which were successfully fabricated with a high degree of uniformity on the TIPS-PEN:PaMS active layer using a simple H-dip solution-coating method. It was shown that bottom-contact TIPS-PEN:PaMS OTFTs prepared with a Cytop/BSA overlayer exhibited higher current flows than those without an overlayer. This high electrical performance of the Cytop/BSA-deposited OTFT was successfully simulated and

interpreted in terms of the formation of dual-current channels in the active layer caused by the electric field effect of the negatively charged BSA overlayer. These OTFTs with high flowing current provide the solid foundation necessary to improve the fabrication of new electrical organic devices, making the use of organic electronic devices possible for a wide range of electrical and biological applications.

Acknowledgements

Notes and references

Department of Electrophysics, Kwangwoon University, Seoul 139-701, Korea. Fax: +82 2943 3208; Tel: +82 2940 5237; E-mail: bcpark@kw.ac.kr

1 H. Sirringhaus, P.J. Brown, R. H. Friend, M. M. Nielsen, K. Bechgaard, B. M. W. Langeveld-Voss, A. J. H. Spiering, R. A. J. Janssen, E. W. Meijer, P. Herwig and D. M. de Leeuw, *Nature,* 1999, **401**, 685.

2 H. E. A. Huitema, G. H. Gelinck, J. B. P. H. van der Putten, K. E. Kuijk, C. M. Hart, E. Cantatore, P. T. Herwig, A. J. J. M. van Breemen and D. M. de Leeuw, *Nature*, 2001, **414**, 599.

3 Z. Bao and J. Locklin, *Organic Field-Effect Transistors (Optical Science and Engineering Series)*, CRC Press, Boca Raton, FL, 2007.

4 H. E. Katz and C. Landis, *Optical Science and Engineering,* 2007, **128**, 403.

5 S. K. Park, J. E. Anthony and T. N. Jackson, *IEEE Electron Device Lett.,* 2007, **28**, 877.

6 D. H. Kim, D. Y. Lee, H. S. Lee, W. H. Lee, Y. H. Kim, J. I. Han and K. Cho, *Adv. Mater.,* 2007, **19**, 678.

7 P. F. Baude, D. A. Ender, M. A. Haase, T. W. Kelley, D. V. Muyres and S. D. Theiss, *Appl. Phys. Lett.,* 2003, **82**, 3964.

8 M. Mizukami, N. Hirohata, T. Iseki, K. Ohtawara, T. Tada, S. Yagyu, T. Abe, T. Suzuki, Y. Fujisaki, Y. Inoue, S. Tokito and T. Kurita, *IEEE Electron Device Lett.,* 2006, **27**, 249.

9 J. A. Rogers, Z. Bao, K. Baldwin, A. Dodabalapur, B. Crone, V. R. Raju, V. Kuck, H. Katz, K. Amundson, J. Ewing and P. Drzaic, *Proc. Natl. Acad. Sci.,* 2001, **98**, 4835.

10 T. Someya, A. Dodabalapur, A. Gelperin, H. E. Katz and Z. Bao, *Langmuir,* 2002, **18**, 5299.

11 F. Yan, S. M. Moka, J. Yub, H. L. W. Chan and M. Yang, *Biosens. Bioelectron.,* 2009, **24**, 1241.

12 L. Kergoat, B. Piro, M. Berggren, G. Horowitz and M.-C. Pham, *Anal. Bioanal. Chem.,* 2012, **402**, 1813.

13 B. Singh, N. S. Sariciftci, J. G. Grote and F. K. Hopkins, *J. Appl. Phys.,* 2006, **100**, 024514.

14 M. Irimia-Vladu, N. S. Sariciftci and S. Bauer, *J. Mater. Chem.,* 2011, **21**, 1350.

15 L. Torsi, M. Magliulo, K. Manoli and G. Palazzo, *Chem. Soc. Rev.*, 2013, **42**, 8612.

16 T. Minamiki, T. Minami, R. Kurita, O. Niwa, S.-I. Wakida, K. Fukuda, D. Kumaki and S. Tokito, *Appl. Phys. Lett.*, 2014, **104**, 243703.

17 T. Minamiki, T. Minami, R. Kurita, O. Niwa, S.-I. Wakida, K. Fukuda, D. Kumaki and S. Tokito, *Materials*, 2014, **7**, 6843.

18 T. Minami, T. Minamiki, Y. Hashima, D. Yokoyama, T. Sekine, K. Fukuda, D. Kumaki and S. Tokito, *Chem. Commun*., 2014, **50**, 15613.

19 M. Medina-Sánchez, C. Martínez-Domingo, E. Ramon and A. Merkoçi, *Adv. Funct. Mater.*, 2014, **24**, 6291.

20 W. Huang, K. Besar, R. LeCover, P. Dulloor, J. Sinha, J. F. Martínez Hardigree, C. Pick, J. Swavola, A. D. Everett, J. Frechette, M. Bevand and H. E. Katz, *Chem. Sci.*, 2014, **5**, 416.

21 Y.-Y. Lin, D. J. Gundlach, S. F. Nelson and T. N. Jackson, *IEEE Trans. Electron Devices,* 1997, **44**, 1325.

22 J. H. Schön, C. Kloc and B. Batlogg, *Org. Electron.,* 2000, **1**, 57.

23 P. T. Herwig and K. Müllen, *Adv. Mater.,* 1999, **11**, 480.

24 M. L. Swiggers, G. Xia, J. D. Slinker, A. A. Gorodetsky, G. G. Malliaras, R. L. Headrick, B. T. Weslowski, R. N. Shashidhar and C. S. Dulcey, *Appl. Phys. Lett.,* 2001, **79**, 1300.

25 T. Fujiwara, J. Locklin and Z. Bao, *Appl. Phys. Lett.,* 2007, **90**, 232108.

26 I. O. Shklyarevskiy, P. Jonkheijm, N. Stutzmann, D. Wasserberg, H. J. Wondergem, P. C. M. Christianen, A. P. H. J. Schenning, D. M. de Leeuw, Ž. Tomovic, J. Wu, K. Müllen and J. C. Maan, *J. Am. Chem. Soc.,* 2005, **127**, 16233.

27 N. Stingelin-Stutzmann, E. Smits, H. Wondergem, C. Tanase, P. Blom, P. Smith and D. de Leeuw, *Nat. Mater.,* 2005, **4**, 601.

28 A. Tracz, J. K. Jeszka, M. D. Watson, W. Pisula, K. Müllen and T. Pakula, *J. Am. Chem. Soc.,* 2003, **125**, 1682.

29 W. Pisula, A. Menon, M. Stepputat, I. Lieberwirth, U. Kolb, A. Tracz, H. Sirringhaus, T. Pakula and K. Müllen, *Adv. Mater.,* 2005, **17**, 684.

30 K. C. Dickey, J. E. Anthony and Y.-L. Loo, *Adv. Mater.,* 2006, **18**, 1721.

31 T. D. Anthopoulos, F. B. Kooistra, H. J. Wondergem, D. Kronholm, J. C. Hummelen and D. M. de Leeuw, *Adv. Mater.,* 2006, **18**, 1679.

32 C.-Y. Liu and A. J. Bard, *Chem. Mater.,* 2000, **12**, 2353.

33 T. Ohe, M. Kuribayashi, R. Yasuda, A. Tsuboi, K. Nomoto, K. Satori, M. Itabashi and J. Kasahara, *Appl. Phys. Lett.,* 2008, **93**, 053303.

34 T. Ohe, M. Kuribayashi, A. Tsuboi, K. Satori, M. Itabashi and K. Nomoto, *Appl. Phys. Express,* 2009, **2**, 121502.

35 B. Park and M. Han, *Opt. Express,* 2009, **17**, 13830.

36 B. Park, H. G. Jeon, J. Choi, Y. K. Kim, J. Lim, J. Jung, S. Y. Cho and C. Lee, *J. Mater. Chem.,* 2012, **22**, 5641.

37 J. Granstrom, J. S. Swensen, J. S. Moon, G. Rowell, J. Yuen and A. J. Heeger, *Appl. Phys. Lett.,* 2008, **93**, 193304.

38 H. U. Khan, J. Jang, J.-J. Kim and W. Knoll, *Biosens. Bioelectron.,* 2011, **26**, 4217.

39 C. Felder and J. Sussman, Protein Dipole Moments Server, Dept. Structural Biology, Weizmann Institute, 761000 Rehovot, Israel, 2007.

40 H. Becker, H. Spreitzer, W. Kreuder, E. Kluge, H. Schenk, I. Parker and Y. Cao, *Adv. Mater.,* 2000, **12**, 42.

41 L. D. Landau and V. G. Levich, *Acta Physicochim. URSS,* 1942, **17**, 42.

42 A. J. Mountford, S. J. Lancaster, S. J. Coles, P. N. Horton, D. L. Hughes, M. B. Hursthouse and M. E. Light, *Inorg. Chem.,* 2005, **44**, 5921.

43 B. W. Matthews, *Encyclopedia of life science,* Nature Publishing Group, 2001.

44 H. U. Khan, J. Jang, J.-J. Kim and W. Knoll, *J. Am. Chem. Soc.,* 2011, **133**, 2170.

45 B. K. Crone, A. Dodabalapur, R. Sarpeshkar, A. Gelperin, H. E. Katz and Z. Bao, *J. Appl. Phys.,* 2002, **91**, 10140.

46 F. Maddalena, M. J. Kuiper, B. Poolman, F. Brouwer, J. C. Hummelen, D. M. de Leeuw, B. De Boer and P. W. M. Blom, *J. Appl. Phys.,* 2010, **108**, 124501.

47 I. Langmuir, *J. Am. Chem. Soc.,* 1916, **38**, 2221.

48 H. R. Farrah and R. F. Steinberg, *IEEE Trans. Electron Devices,* 1967, **ED-14**, 69.

49 G. H. Gelinck, E. van Veenendaal and R. Coehoorn, *Appl. Phys. Lett.,* 2005, **87**, 073508.

50 J. E. Northrup and M. L. Chabinyc, *Phys. Rev. B,* 2003, **68**, 041202.

51 D. Feili, M. Schuettler, T. Doerge, S. Kammer and T. Stieglitz, *Sens. Actuators A,* 2005, **120**, 101.

52 CHARMM-GUI, http://www.charmm-gui.org/, accessed 2006.

53 W. Im, D. Beglov and B. Roux, *Comput. Phys. Commun.,* 1998, **111**, 59.

54 Silvaco International, ATLAS User's Manual, SC, 2000.

55 A. E. Wiącek and E. Chibowski, *Colloids and Surfaces B: Biointerfaces*, 2002, **25**, 55.

Table 1. Summary of the device performance of OTFTs investigated in air.

Overlayer(s)	Effective mobility ($cm^2V^{-1}s^{-1}$)	On/off ratio [b]	Threshold voltage (V)
W/O (reference)	0.20±0.02 (0.22) [a]	3.97×10^4 (1.57×10^4)	-1.62±11.91 (-16.87)
Cytop	0.22±0.03 (0.26)	1.10×10^5 (3.35×10^4)	-0.10±10.40 (-14.73)
Cytop /BSA	0.25±0.05 (0.31)	1.41×10^5 (4.89×10^4)	1.26±9.08 (-12.18)
BSA	0.24±0.03 (0.29)	1.81×10^5 (3.75×10^4)	-2.07±4.41 (-0.62)

[a] The number in parentheses in each cell is the maximum value from the observations; [b] when V_{DS} = -60 V.

Table 2. Summary and comparisons of the sensor performance of pentacene-based OTFTs investigated in solutions.

	Active layer	Averaged mobility (±SD) ($cm^2V^{-1}s^{-1}$)	Sensing materials	Limit of detection	Range of response
Our work	TIPS-PEN:PaMS	0.20 (±0.02)	BSA	1.2 μM	500 nM ~ 100 μM
Ref 10	Pentacene	-	Lactic acid, glucose	-	10 μM ~ 2 mM
Ref 20	Pentacene	0.07 (±0.01)	GFAP	20 pM	0.8 ~ 400 ng/ml
Ref 38	Pentacene	5.4×10^{-3}	antiBSA	-	-
Ref 44	Pentacene	0.12	antiBSA	-	10 nM ~ 2 μM

Table 3. Summary of the parameters used in the OTFT simulations.

Simulation parameters [a]	TIPS-PEN	Cytop	BSA
Permittivity	4.0	2.0	2.1
Energy Band Gap [eV]	3.2	-	-
Electron Affinity [eV]	5.5	5.0	-
P-type doping in active layer [$\times10^{15}$]	4.8	5.2	5.2
Mobility of active layer [$cm^2V^{-1}s^{-1}$]	0.2	0.2	0.2
Surface charge density [$\times10^{10}cm^{-2}$]	-	-	-4.0

[a] The density of states of the effective valence band and the conduction band of TIPS-PEN were set, respectively, to 2.5×10^{25} cm^{-3}.
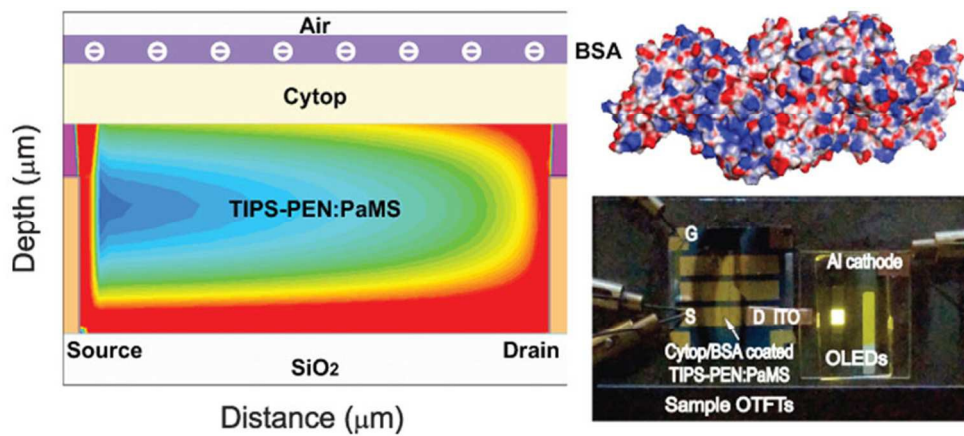
Organic thin-film transistors with insulator/protein overlayers are successfully fabricated by employing negatively charged protein overlayers to achieve high-performance devices.
80x34mm (300 x 300 DPI)